

FASCIA STRESS PATTERNS ARE HIGHLY DEPENDENT ON TISSUE STRUCTURE

Vickie Shim¹, Benjamin Fischer², Jörg Böhme¹, Hanno Steinke², Sascha Kurz²
¹Auckland Bioengineering Institute, University of Auckland, ²ZESBO, Leipzig University

INTRODUCTION

Fascia plays an important role in musculoskeletal dynamics: stiffness of pantar-fascia contributes to the stability of the foot and the lumbar fascia limits spinal mobility. Recent studies showed fascia can adjust its stiffness to contribute actively to musculoskeletal dynamics[1]. Here we present a novel system that combines experimental and modeling approach. Specifically we have performed mechanical experiment on human fascia tissues and then created finite element (FE) models of the tissue to analyze fascia tissue biomechanics.

METHOD

Fresh-frozen samples of human thoracolumbar fascia were prepared for the experiments. After thawing, the main collagen fiber direction of the fasciae tissue, orientated to the latissimus dorsi muscle, was determined. Tensile testing of the tissue samples in this fiber direction was performed accordingly. For this, the samples were cut to rectangular strips with a length of 60 mm and a width of 10 mm. Thus, the main fiber direction was parallel to the direction of the tensile test. The clamping areas of the samples were dehydrated with acetone (20 min) and plastinated with a compound of polyurethane resin and aluminium hydroxide (20 min plastination time), which infiltrated the dry tissue, resulting in a hard and firm connection between tissue and resin. To further improve the grip of the clamps, thin slices of beech wood were also integrated into the resin compound. The middle part of the samples was protected from acetone and resin by covering with aluminium plates from both sides, only exposing the clamping areas to acetone and resin. Tensile testing was performed with a deformation velocity of 5 mm min⁻¹ and a preload of 5 N until sample failure occurred. FE models of those samples were generated. We used the mutually-orthogonal curvilinear material coordinate system in our FE models and aligned it according to the fiber orientations of the fascia tissue used in the experiment using a previously validated fibre fitting procedure [2]. Transversely isotropic material properties were used with material parameters obtained from our previous study [3]. The same uniaxial stretch was applied to the model until failure. The failure pattern observed in the experiment was compared with the model predicted patterns.

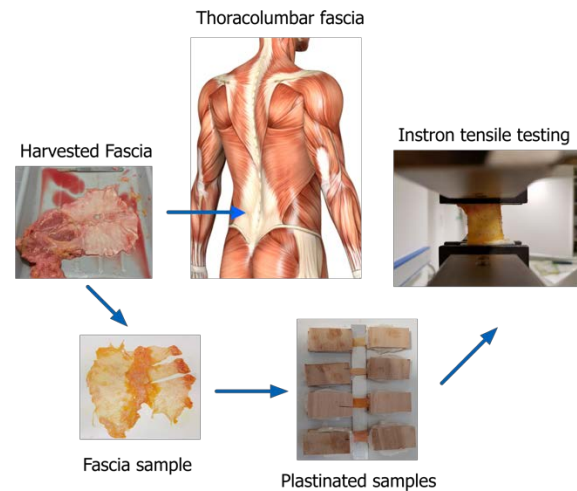


Figure 1. Experimental framework

RESULTS & CONCLUSION

Fascia tissue samples failed on average at 172.46N. A clear vertical rupture line appeared in the direction of load application. When run with the same loading condition as the experiment, our model predicted the similar rupture pattern (Figure 2), giving us confidence in model performance. This novel system that combines both experimental and modelling approaches will be used to identify the structure-function relationship in fascia.

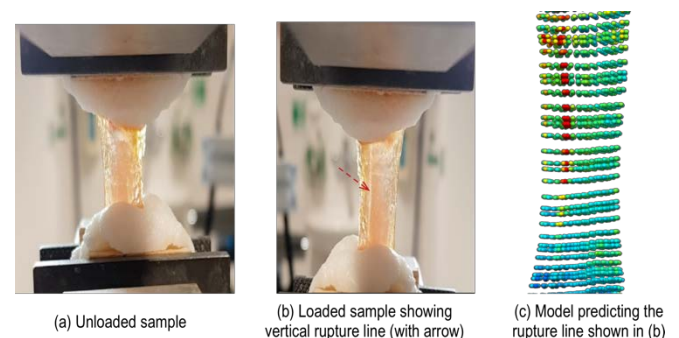


Figure 2. Results comparing experimental and modelling results.

REFERENCES

- [1] Schleip et al. Med. Hypo. 2005;62(2):273-277
- [2] Shim VB et al. Biomech Model Mechanobiol. 2016;15(1):195-204.
- [3] Shim VB et al. Journal of Biomechanics. 2014;47(15):3598-604

DESIGN AND MANUFACTURING OF A LOW-COST ROBOTIC ANKLE FOR INDONESIAN TRANS-TIBIAL AMPUTEES

F. Ferryanto¹, Edgar B. Sutawika¹, Sandro Miharadi¹, Tatacipta Dirgantara², Indrawanto³,
Haridhi Dzar Tazakka¹, Andi Isra Mahyuddin¹

Faculty of Mechanical and Aerospace Engineering, Institut Teknologi Bandung
Jalan Ganesa 10, Bandung 40132, INDONESIA

Corresponding author email: aim@ftmd.itb.ac.id

INTRODUCTION

Increased number of motorcycle accidents in Indonesia in the last several years have resulted in many amputations. Unfortunately, most of these amputees are young and come from low-income families. Affordable prosthetics are needed to enhance their mobility. The issue with current simple prosthetics for lower extremity amputees is the inability to produce positive work to propel the body forward during push-off. As a result, the gait of amputee is asymmetric and could cause pain in the knee and/or hip joints. Furthermore, the design of commercially available prosthetics is not based on Indonesian gait parameters and most are prohibitively expensive. Hence, the aim of this work is to design an affordable robotic ankle prosthetic to match the normal Indonesian gait parameters for trans-tibial amputees.

METHOD

In the present work, a prosthetic ankle design known as SPARKy (Spring Ankle with Regenerative Kinetics) [1] was selected as the reference to design a robotic ankle prosthetic compatible with Indonesian gait parameters. The main different of the proposed design would be the utilization of Indonesian gait data which has a smaller mechanical power output at the ankle compared to European gaits. The material of energy storage & return (ESAR) keel is modified to aluminum due to its lower cost, availability, and manufacturability.

There are four important functional parameters for the robot ankle prosthetic considered, i.e. the DC motor gearbox ratio, leadscrew pitch, robotic tendon spring stiffness, and ESAR foot lever length. The optimal combination of the parameters is determined to maximize the system's efficiency to achieve the smallest electrical energy required for one gait cycle.

RESULTS AND DISCUSSIONS

By iterations, the optimum parameters found are (1) a gearbox ratio of 1:3.7, (2) an 8-mm lead screw with a pitch of 4 mm/revolutions, (3) spring stiffness of 33.000 N/m, and (4) lever length of 9 cm. With these prosthetic parameters, the required energy per walking

step is 54 Joules. A Maxon RE-32 24V DC motor is suitable for the requirements.

The 3D model of the robotic ankle is shown in Figure 1. Next, a manufacturing analysis will be conducted, which may result in minor modification of the design. Manufacturing processes mainly will be forming and machining, and would be optimized to reduce costs.

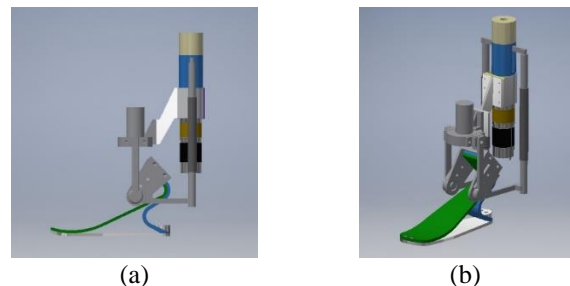


Figure 1. (a) Isometric and (b) side view model of the proposed design of robotic ankle

CONCLUSIONS

A robotic ankle prosthetic has been designed based on SPARKy with features that include the use of Indonesian gait parameters and an affordable aluminum keel with similar capabilities with commercial keels. Four important parameters for the mechanical design has also been determined while considering component availability. The active ankle prosthetic is powered by a Maxon RE-32 24V DC motor.

ACKNOWLEDGEMENTS

The authors gratefully acknowledge the support from Ministry of Research Technology and Higher Education who have made this work possible through *Penelitian Terapan Unggulan Perguruan Tinggi* scheme research grant for year 2018.

REFERENCES

1. Hitt, Joseph K., et al., Journal of medical devices 4.1, 2010.
2. Miharadi, S. et al., Eighth Asian-Pacific Conference on Biomechanics, 2015

Speaker: Andi Isra Mahyuddin, aim@ftmd.itb.ac.id

RELIABILITY AND SENSITIVITY OF RADIOGRAPHIC OUTCOME MEASURES FOR HIP DYSPLASIA IN PAEDIATRIC CHARCOT-MARIE-TOOTH DISEASE

Leanne Purcell^{1,2}, Paul Gibbons^{1,2}, Kamal Jamil^{1,3}, David Little^{1,2}, Oliver Birke^{1,2}, Manoj P Menezes^{1,2}, Joshua Burns^{1,2}

(1) Sydney Children's Hospitals Network (Randwick and Westmead), Australia

(2) University of Sydney, Australia

(3) Universiti Kebangsaan, Kuala Lumpur, Malaysia

INTRODUCTION

Hip dysplasia describes disruption of hip and acetabular alignment and congruency, with severity ranging from mild subluxation in 'at risk' hips, to complete dislocation. Onset of neurological hip dysplasia can be sub-clinical, with varied clinical presentation such as a limp with or without hip pain, abductor and flexor weakness, reduced hip range of motion, and even asymptomatic in some cases. The incidence of hip dysplasia in children with Charcot-Marie-Tooth disease, the most common inherited neuropathy, has been reported to be ~8%, however a recent case series has suggested that it may be closer to 20%. Hip dysplasia can be detected using radiographs, however there is limited evidence for the reliability of current measures. Therefore, the aim of this study was to identify reliable radiographic measures of hip dysplasia in paediatric Charcot-Marie-Tooth disease, and describe the cohort's hip health relative to normative reference data to further understand the presentation and biomechanical implications of affected children.

METHOD

We identified 30 children from the Australasian Paediatric Charcot-Marie-Tooth disease Registry who had an anteroposterior pelvis x-ray. Fourteen radiographic measures of hip dysplasia were identified from the literature, and were scored independently by two orthopaedic surgeons (one senior and one junior). The senior surgeon also categorised the hip health of the 30 children based on clinical impression (at-risk or non- dysplastic).

Intraclass correlation coefficients were calculated to assess the reliability of the 14 radiographic measures.

RESULTS

Eight measures (acetabular index, centre edge angle, neck shaft angle, medial joint space, head width, lateral uncoverage, migration percentage and triradiate status) were found to be reliable between the 2 assessors (ICC >0.75 between raters). Five of the 30 children with Charcot-Marie-Tooth disease (17%) were identified as having hips 'at risk' of hip dysplasia. Reliable radiographic measures that significantly distinguished between 'at risk' and 'non-dysplastic' hip health are shown in Table 1.

CONCLUSIONS

We have identified the most reliable measures of hip alignment and the most sensitive measures of hip health in children with Charcot-Marie-Tooth disease. These measures could be used to screen affected children during childhood and adolescence to mitigate the deleterious effects of hip dysplasia and related gait difficulties and chronic pain in adulthood.

REFERENCES

- Kumar, S. J Paed. Orthop. 5, 511-514, 1985.
Eklof, O. Acta Radiologica. 29(3), 363-366, 1988
Gdalevitch, M. J Peripher Nerv Syst. 20, 47, 2015.

Email: leanne.purcell@sydney.edu.au

Table 1. Reliable radiographic measures that distinguished between 'at risk' and 'non- dysplastic' hip health

	Reliability (n=30)		At Risk (n=5)	Non-Dysplastic (n=25)	Difference
	ICC	95% CI	Mean (SD)	Mean (SD)	p-value
Lateral Centre Edge Angle (°)	0.84	0.69 – 0.92	21 (5)	33 (7)	0.001
Migration Percentage (%)	0.83	0.68 – 0.92	20 (5)	12 (6)	0.01
Medial Joint Width (mm)	0.80	0.62 – 0.90	6.9 (1)	4.9 (1)	0.001
Acetabular Index (°)	0.76	0.19 – 0.92	16 (4)	11 (4)	0.02

RIGHT-TO-LEFT SHAPE DIFFERENCES IN THE ULNA

Desney Greybe¹, Julia Reinstein¹ and Michael Boland^{1,2}

1. Auckland Bioengineering Institute, University of Auckland, New Zealand.

2. Hand Institute, Auckland, New Zealand.

INTRODUCTION

Ulnar fractures account for 10% of all fractures treated in publicly-funded New Zealand hospitals [1]. Poorly healed fractures of the forearm have severe consequences for upper limb function. Consequently, a quarter of all ulnar fractures require corrective surgery. There is an increasing move towards patient-specific, computer-assisted approaches to surgical planning, with the contralateral bone used as a model of the pre-injured ulna [2]. However, this approach assumes that right and left ulnas are essentially identical in shape. The validity of that assumption is unknown. The goal of this study was to investigate shape differences between left and right ulnas. Bone shape was evaluated using a statistical shape model.

METHOD

The left and right ulnas of 35 individuals were segmented from postmortem computed tomography data (1x1x1 mm). The bone models were registered using eigenvectors, with the left mesh reflected to match the right. All bone meshes were scaled isotropically to the same length, so that subsequent analysis considered only differences in shape. Non-rigid registration of a triangular surface mesh was performed using radial basis functions, providing bone meshes with nodal correspondence. Principal component analysis was performed on the normalized bone meshes to determine the independent modes of variation that existed within the data set. The absolute difference in mode weight between left and right ulnas was calculated relative to the standard deviation (SD) of weights across the population.

RESULTS

The first six principal components captured 92% of the total shape variation, having normalized bone length.

The first mode, which primarily represented a change in volume, accounted for 49% of the variation. On average, there was a 1.2 ± 0.9 SD difference in the mode weight between the left and right ulnas.

The second mode primarily captured a change in the curvature of the ulna. A negative mode weight corresponded with a “C” shaped bow, while a positive mode weight produced an “S” shaped bow through bending at the distal ulna. This mode accounted for 13% of the shape variation across the population. On

average, the left ulna differed from the right by 1.1 ± 0.9 SD in this mode of variation.

The third mode captured longitudinal rotation of the ulnar shaft and accounted for a further 12% of the shape variation. On average, the right and left ulnas differed by 1.1 ± 0.8 SD in this mode.

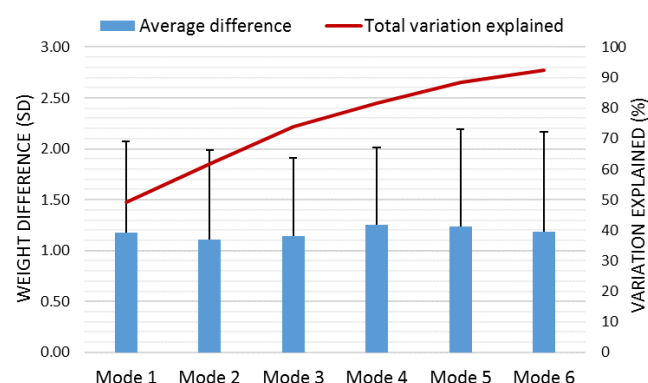


Figure 1. Average difference in mode weight between left and right ulnas and the percentage of shape variation explained by the first six principal components.

CONCLUSIONS

On average, the right ulna differed from the left by more than 1 SD in each of the first six modes of shape variation. These results do not support the assumption that left and right ulnas are essentially equivalent in shape. Therefore, further study is warranted. Half of the variation in ulnar shape is associated with volume differences, which makes sense given its load-bearing role in the forearm. The second and third modes of variation represented changes in the shape of the ulnar shaft and may be important for forearm rotation. In future research, it will be necessary to evaluate the functional significance of these shape differences.

ACKNOWLEDGEMENTS

Victorian Institute of Forensic Medicine
Lottery Health Research
Otto Helmut and Alice Eckl Foundation

REFERENCES

1. Ministry of Health, 2011-2012.
2. Miyake, J. J Bone Joint Surg Am. 94, e150, 2012.

PRESENTER

Desney Greybe, dgre057@aucklanduni.ac.nz

CLUSTERING HEALTHY RUNNER BASED ON 3-D KINEMATICS PATTERNS OF PELVIC DURING RUNNING USING HIERARCHICAL METHOD

Davood Khezri¹, Mansour Eslami², Roholah Yosefpor³

1. Ph.D. Candidate in sport biomechanics 2. Associate prof, of sport biomechanics 3. Associate prof, of Mathematics and Statistics

INTRODUCTION

Running injury pertaining to pelvic accounted for approximately 11 to 13 of all injury sustained. The overuse injuries epidemiology to this region in the runner are not as common as in the lower limb (1,2). However, several case studies have highlighted that overuse injuries of the lumbar spine and pelvis can frequently be debilitating requiring prolonged periods of rehabilitation.

It has been reported that the main causes of these injuries is excessive motions in pelvic (3). However, the normal range of motion in pelvic is not clear until now. In the past literature, pelvic ROM is too wildness (3, 4). Probably, causes of this wideness is existence homogenous groups in healthy papulation based on pelvic motion. The hierarchical method was used for clustering runner based on limbs motion (5). Therefore, the aim of this study is clustering runner based on pelvic motions by the hierarchical method and investigate the pelvic motions difference between finding groups.

METHOD

3-D kinematics of pelvic of ninety healthy young runners were recorded during running by four Basler video camera. Participant ran at self-selected speed on treadmill for 3-minuts. 10 gait cycle was chosen for analyses. Joint angle normalized by 100. Principle component analysis was used for data dimension reduction. Fore finding homogenous groups, hierarchical method was applied. The validation of clustering was confirm by inconsistency coefficient. The effect size of 0.80 and alpha of 0.05 was chose as significant threshold.

RESULTS

Result showed that two homogenous groups with 36 and 54 subjects are exist in all runners based on pelvic motions. The major difference in pelvic motion between groups was in sagittal and transverse plane (fig 1).

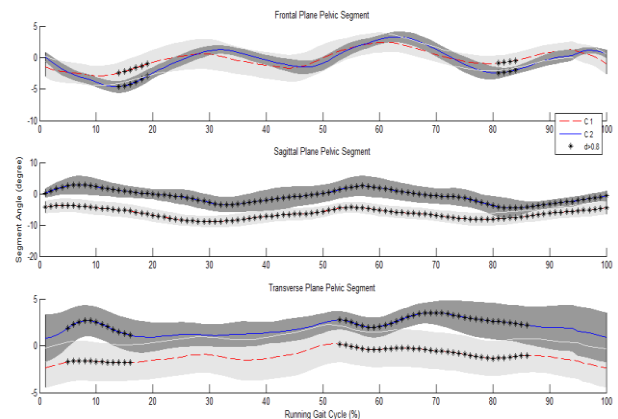


Figure 1. Pelvic angle in two groups, discrete and continues line showed the cluster 1 and 2. * showed significant difference between groups.

CONCLUSIONS

Finding healthy homogenous groups based on pelvic motions and difference of it between groups is useful for correct interpretation of pelvic movement during running (specifically wideness in pelvic ROM), rooting of running injury and their rehabilitation.

REFERENCES

1. Schache AG, Blanch P, Rath D, Wrigley T, Bennell K. Human movement science, 2, 273-93, 2002
2. Koch RA, Jackson DW. The American journal of sports medicine, 9, 62-3, 1981
3. Laird RA, Gilbert J, Kent P, Keating JL. BMC musculoskeletal disorders, 15, 1-13, 2007
4. Ellis R, Hing W, Reid D Manual therapy, 12, 200-208, 207
5. Phinyomark A, Osis S, Hettinga BA, Ferber R. Journal of biomechanics, 48, 3897-3904, 2014

Speaker's name: Davood Khezri , Mansour Esalmi

Email address: D.khezri@stu.umz.ac.ir

KINEMATIC STUDY OF CLEAN AND JERK LIFT IN THE 69-KG CATEGORY WEIGHTLIFTING

Tommy Apriantono^{1*}, F. Ferryanto², Indria Herman², Richard Anderson¹, Erich Adyawibawa Soemantri¹

¹Sport Science Research group, School of Pharmacy

²Mechanical Design Research Group, Faculty of Mechanical and Aerospace Engineering

Institut Teknologi Bandung

Jalan Ganesa 10, Bandung 40132, INDONESIA

*Corresponding author email: tommv@fa.itb.ac.id

INTRODUCTION

Weightlifting is one of a prominent sport in Indonesia because there were 10 Olympic medal from this sport since 2000 Sydney Olympic. Most of the weightlifting Medalist participated in the 69-kg category or lower. Furthermore, all Indonesia's Olympic Medalist have lower than 1.70 meter height. This facts also apply for top five rank in the 2016 Rio Olympic for the 69-kg category or lower [1]. Hence, the anthropometry of the weightlifters may have a correlation with the category that they participate. The effect of height to the performance of weightlifter has been studied by Storey and Smith in general, but not biomechanically [2].

The main objective of this work is to study the correlation of the weightlifter anthropometry to the kinematic and kinetic parameters as the preparation for the Tokyo Olympic in 2020. As the preliminary study, this paper presents the kinematic study of the clean and jerk lift in 69-kg weightlifting category.

METHOD

Experiments to obtain weightlifting motion is conducted by Simi Motion 3D which consists of four cameras with speed 200 frames per second. Markers are attached on 14 anatomical position shown in Figure 1. Then, hip, knee, ankle, shoulder and elbow angle are calculated from the 10 participants that performed clean and jerk at 85% of one repetition maximum (1RM). In addition, the Ground Reaction Force (GRF) of the participants was acquired by force platform AMTI Accu Power.

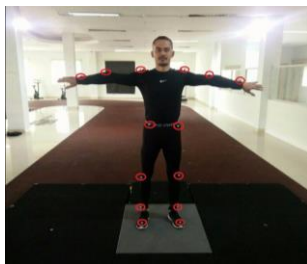


Figure 1 Marker position attached on the participant

The participants was selected based on their weight and height. The weight of the participants should be in

the 69-kg category weightlifting, i.e. between 62 kg and 69 kg. The participants are divided into two groups according to their heights, i.e. lower than 1.68 meter and higher than 1.73 meter.

RESULTS

Figure 2 shows example of kinematic parameters in this preliminary study, i.e. left and right hip angle of clean and jerk lift. The right and left hip angle are asymmetrical. The completion of the clean phases took 4.02 s while the jerk phases took 0.856 s. Both phases involves explosives move of the hip.

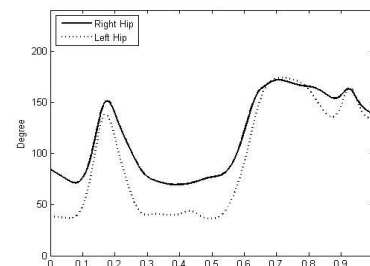


Figure 2. Hip angle

CONCLUSIONS

Optical motion capture with 14 markers and four cameras has been used to obtain the motion of clean and jerk lift. Ten participants with two height groups who are in the 69-kg category weightlifting participate in this work. Kinematic parameters is then obtained, e.g. hip angle. The completion of the clean phases took 4.02 s while the jerk phases took 0.856 s.

ACKNOWLEDGEMENTS

The authors gratefully acknowledge the support from ITB for the *Program Penelitian, Pengabdian kepada Masyarakat, dan Inovasi* (P3MI) KK ITB 2018 research grant and *Rumah Sakit Olahraga Nasional* for the Simi Motion facility.

REFERENCES

1. IWF, 2018, <http://www.iwf.net/results/results-by-events/?event=362>
2. Harbili, E. *J Sports Sci Med* 11, 162-169, 2012.

Speaker: Ferryanto, ferryanto@fmd.itb.ac.id

The effect of strengthening the muscles of the foot on common ligament injury mechanism in females participating in court sports.

Carla van der Merwe^a, Sarah P Shultz^b, Bob GR Colborne^c, and Philip W Fink^a

^a School of Sport, Exercise and Nutrition, Massey University, Palmerston North, New Zealand; ^b School of Sport, Exercise and Nutrition, Massey University, Wellington, New Zealand; ^c School of Veterinary Science, Massey University, Palmerston North, New Zealand

Introduction

Court games are characterised by rapid and repetitive short bursts of multiplanar accelerations and decelerations. Abrupt, unanticipated changes of direction put participants of court sports at an increased risk for sustaining non-contact anterior cruciate ligament ruptures (ACL) and lateral ankle sprains (LAS). ACL and lateral ankle sprain injury mechanism research suggest that foot mechanics play a key role, but very few intervention programs aim to change foot function directly. The aim of this project is therefore to investigate the effect that the strengthening of specific muscles of the foot and lower leg will have on the injury mechanism associated with ACL and lateral ankle sprain injuries. To test the efficacy of the muscle strengthening program, sixteen female court sport athletes were randomly assigned to either an intervention group or a control group. Both groups were given a pretest consisting of vertical jumps (VJ) and 45 degree unanticipated cutting movements (UAC). The intervention group then took part in a 16-week progressive foot muscle-strengthening program three times a week. Following the intervention, both groups were tested again on the VJ and UAC. Preliminary results showed an improvement in performance measures (vertical jump height, stance time, deceleration time) and injury risk factors (knee valgus angle and knee and ankle ground reaction force moment arms), indicating that muscle strengthening programs targeting the foot musculature could play a role in reducing injuries in court sports.

RAPID QUADRUPEDAL LOCOMOTION

Hasti Hayati, David Eager, Paul Walker

School of Mechanical and Mechatronic Engineering, Faculty of Engineering and IT,
University of Technology Sydney (UTS)

INTRODUCTION

Locomotion means moving from one place to another and gait is specific patterns of locomotion. Galloping gait is the fastest gait but the most fatiguing one in quadrupeds such as greyhounds. To study the impact of compliant terrains (natural grass and synthetic rubber) on the biomechanics of rapid legged movements, a well-known spring loaded inverted pendulum (SLIP) model is deployed. The model is a three-degrees-of-freedom (3-DOF) system inspired by galloping greyhounds. The single support phase of the hind-leg stance event, in a galloping gait, is taken into consideration. The rationale of modelling hind-leg was its high rate of musculoskeletal injuries [1] as well as its primary function in powering the greyhound's locomotion [2].

METHOD

To set the initial conditions, high frame rate videos of racing greyhounds galloping on a straight section of a track were analysed (Fig.1.A). The spring and damping coefficient of terrains (Fig.1.C) have been conducted by analysing the load-deformation plots of a conducted drop test.

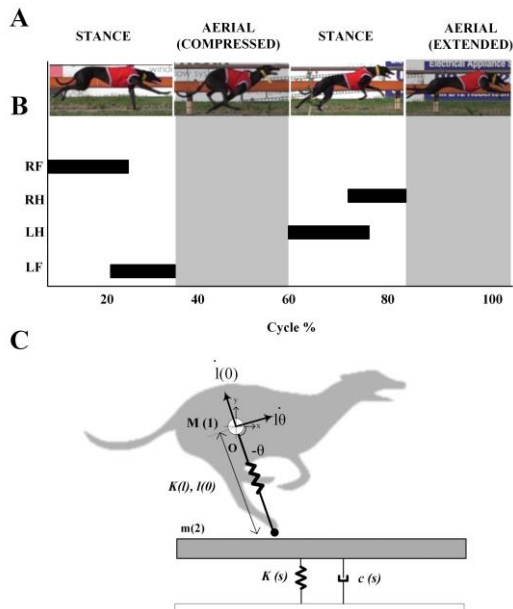


Figure 1. Galloping greyhound (A). Footfall timing of each leg in the gait (B). SLIP model of hind-leg stance and underneath terrain (C).

The Lagrangian method has been deployed to obtain the equation of motion. The nonlinear second-order

differential equations of motion have been numerically solved using Runge-Kutta method in MATLAB R2017b.

RESULTS

The model could predict greyhound's muscle force required to gallop on grass, rubber and ideal case (rigid terrain). The results showed that the required muscle effort for gallop on grass surface not only had higher peaks (4900 N) but also had longer duration compared to rubber (4800 N) and ideal case (4600 N). High ground reaction forces values are one of the main reason of injuries in other sports and activities [3].

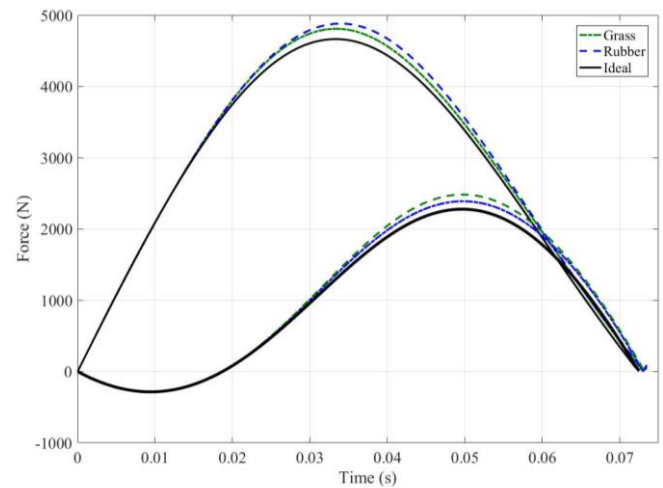


Figure 2. Ground reaction forces of galloping on grass, rubber and rigid terrain.

CONCLUSIONS

The result of this study is essential for the safety and welfare of racing greyhounds by identifying optimum athletic track properties to reduce risk of catastrophic injuries. This research is expandable to other sports such as equine racing. Moreover, it's useful in bio-inspired engineering and robotics in designing legged machines.

REFERENCES

Hayati, H. Eager, D. Stephenson, R. Brown, T. Arnott, E. 9th Australasian Congress on Applied Mechanics, 2017.

Usherwood, J.R. Wilson, A.M. Nature 438, 753-754, 2005.

Hayati, H. Eager, D ASCE-ASME Journal of Risk and Uncertainty in Engineering doi:10.1115/1.4039999, 2018.

Hasti Hayati; Hasti.hayati@uts.edu.au

NON-INVASIVE ESTIMATE OF LEFT VENTRICULAR PRESSURE USING ULTRASOUND

Amila Hasantha Perera¹, Kat Gilbert³, Andrew Lowe², Martyn Nash¹

¹Auckland Bioengineering Institute, University of Auckland, New Zealand

²IBtec, Auckland University of Technology, New Zealand

³Faculty of Medical and Health Sciences, University of Auckland, New Zealand

INTRODUCTION

Blood pressure recordings are among the most frequently used parameters in clinical practice to assess cardiovascular status, performance and disease. At present, the only way to accurately measure pressure in the left ventricle is invasively, via catheterisation. This project aims to investigate the viability of using blood pressure recordings in conjunction with Doppler ultrasound images as a non-invasive surrogate for catheterisation recordings. Echocardiography is the workhorse of cardiac imaging and is widely available. The study explores to determine the non-invasive measurement estimation of the left ventricular (LV) cavity during cardiac cycle that will be validated using (invasive) catheterisation recordings. This consists of collecting both non-invasive pressure measurements (using Uscom BP+ recordings) as well as invasive pressure measurement (catheterisation recordings), and echo images in patients with aortic regurgitation.

METHODOLOGY

The initial stage of this study consisted of the literature review that was performed to understand and analyse the state-of-the-art methods used for estimating LV pressure based on ultrasound and MRI data. This study will validate the reliability and accuracy of the LV pressure measurements using the Simplified Bernoulli equation (SBE) which is the most ubiquitous in clinic [1]. The second stage of this project consists of an experimental study, where flow and pressure through different orifices are examined in a continuous flow setup as well as, in a pulsatile flow setup. For this, the flow was examined through a venturi tube, different orifice plates as well as a percutaneous heart valve. Continuous wave Doppler imaging will be used and the velocity recordings will be converted to pressure gradient recordings using SBE. This will be validated using Miller catheters that will be inserted within both setups (Figure 1). The pressure loss through the orifices and their respective amounts of pressure recovery will be considered in the SBE [2]. The third stage of this study, ultrasound images (Figure 2) and Uscom BP+ cuff recordings from patients at Auckland City Hospital will be obtained and analyzed (ethics and protocols are already approved).

FUTURE WORK

This clinically obtained data set of Doppler images will be combined with the Uscom BP+ estimates of aortic pressure to provide LV pressure traces throughout the entire heart cycle. The gathered experimental data and their modelling assumptions will be applied to the clinical data set. A prototype software tool will be developed to provide LV pressure estimates in the clinical settings. This will be validated using the clinical invasive catheterization. This tool will be designed and tested with regular input from our clinical collaborators, to integrate with existing clinical workflows.

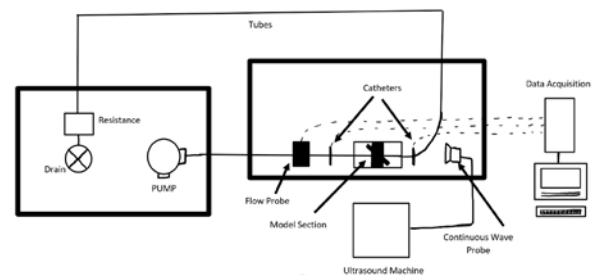


Figure 1: Continuous flow set-up.

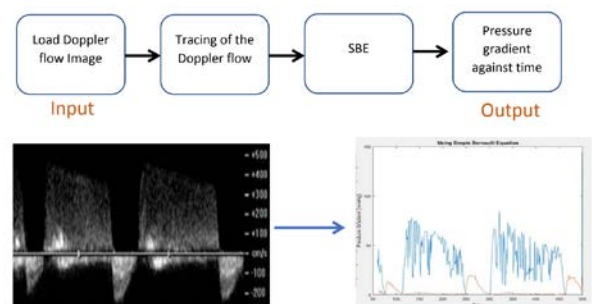


Figure 2: Obtaining Pressure gradient by using SBE to the Doppler image.

REFERENCES

- [1] Bertoglio et al. International journal for numerical methods in biomedical engineering, 34(2): e2925, 2018
- [2] Heinrich et al. Annals of biomedical engineering, 24(6): p. 685-694, 1996

Speaker – Amila Hasantha Perera,
mper509@aucklanduni.ac.nz

Safe Lifting Ergonomics Program for Truck-Loaders: A Multi-site Case Study with Qualitative and Econometric Analyses

Adeyemi H. Oluwole

Department of Mechanical Engineering, Olabisi Onabanjo University, Agoiwoye, Nigeria
adeyemi.hezekiah@oouagoiwoye.edu.ng,

ABSTRACTT

BACKGROUND: An ergonomics method of lifting (EML) was introduced to truck loaders in the South-western Nigeria blocks-making industry(BMI). The aim was to measure the ergonomics and economic benefits.

METHODS: With 125 workers and 30 managers from 25 BMI, workers' self-adopted un-ergonomics methods of lifting (UML) were assessed at baseline. Workers then received ergonomics training. Actual lifting time, pace/time losses, task quality were measured pre and post-intervention in addition to a cost evaluation, at the 7th, 30th and 60th days into EML implementation, involving return-on-training-investment (ROTI) and ergonomics training-yield index (ErgoT-YI). Job demands and workers/managers' opinions about UML and EML were rated through questionnaires.

RESULTS: Under UML, 76% of the workers frequently were absent from work due to lifting-related injuries of which 84% complained of fatigue, back and shoulder pains. Performance under UML was 64% and rated 48% after EML implementation. The average actual productive time improved from 95% (UML) to 97% (EML). $ROTI_{EML}$ was better than $ROTI_{UML}$ by 18.5%. The calculated ErgoT-YI was 1.18 after 7days post-intervention and increased to 18.62 after 60 days, making EML superior to UML. An independent samples *t*-test showed a reduction in product/material wastage with EML ($t = 7.900$; $p < .01$, $SED=108.35$). Other benefits included reduced medical costs and absenteeism by 98.3% and 66.7% respectively.

CONCLUSION: EML can be a cost-effective way to benefit the health and wellbeing of truck loaders, but that supervisors and workers may need to be informed of the economic benefits of this approach in order for it to be fully accepted.

SENSOR VALIDATION OF A SMART KNEE BRACE

A Alder¹, D Wells², P. A. Hume² and A McDaid^{1,3}

¹University of Auckland, ²Auckland University of Technology, ³OPUM Technologies Ltd

INTRODUCTION

Knee braces are often prescribed to patients recovering from knee surgery [1]. Presently, surgeons and clinicians organize in-person appointments to manually assess their patients' recovery. Typically this includes recording clinical measures such as active range-of-motion (AROM). However, a smart knee brace with integrated sensors, such as the Digital KneeTM (Figure 1), may provide automated and objective clinical insights and hence reduce the need for lengthy appointments. To determine the systematic accuracy of the Digital KneeTM it was compared with a "gold standard" VICON optical motion capture system.



Figure 1. Digital KneeTM.

METHODS

A pilot study was conducted in two stages. The first stage involved the manipulation of the brace through its full 150° range-of-motion in an ad-hoc trajectory for 50 s where VICON marker clusters on the brace arms allowed for direct comparison between both measurement systems. In the second stage the brace was worn by a healthy male subject and marker clusters were placed on the participant's leg according to the University of Western Australia (UWA) marker protocol [2, 3]. Two tests were then performed: (a) 30 seconds of treadmill walking and (b) AROM assessment. Both tests were conducted with different configurations and imperfect alignments as may be expected by an at-home unsupervised user, to replicate the best- and worst- case brace situations. The different conditions were: (1) sensor taped directly to leg; (2) sensor fixed to the brace; sensor attached to brace using Velcro sleeve with initial brace alignment to knee, (3) aligned, (4) hyper-extended and (5) hypo-extended.

RESULTS

The correlation of the two measurement systems independent of a wearer (stage 1), showed a mean absolute difference (MAD) of 1.39° and a Root Mean Square Difference (RMSD) of 1.86°. The MAD and RMSD for stage 2 (Table 1) demonstrated differences between the measurement systems for recording

human knee angle, where brace error was intentionally introduced with different alignment conditions. During condition 1 the brace and motion capture angles are always within 3.5° (Figure 2), which is within the motion capture methods declared systematic error range [2].

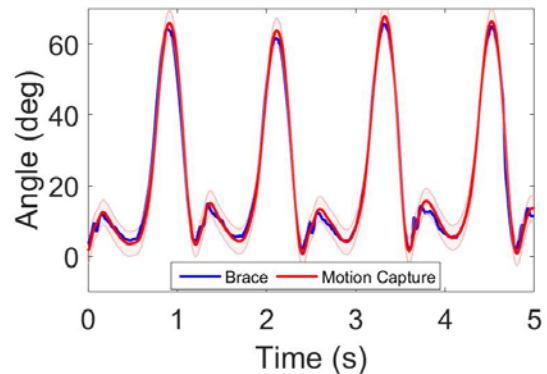


Figure 2. VICON motion capture and brace data

Table 1. MAD and RMSD for Stage 2

Condition Number	Test 2a (°)		Test 2b (°)	
	MAD	RMSD	MAD	RMSD
1	1.36	1.83	2.07	2.97
2	3.71	5.35	2.89	3.34
3	5.35	6.33	2.19	2.81
4	4.53	6.14	4.46	5.18
5	4.27	5.69	5.71	6.84
Average	3.84	5.07	3.46	4.23

Condition 1 showed the best results with a MAD of 1.36° and a RMSD of 1.83°, which is comparable to the sensor only case in stage 1. As expected condition 5 was the worst with MAD of 5.71°. The difference in MAD due to alignment of the brace was 4.35°.

CONCLUSIONS

The knee brace with integrated sensors demonstrated clinically comparable results with the VICON motion capture system for determining knee angles even when intentionally misaligned.

REFERENCES

- [1] Lowe, W, Warth, R, Davis, E, Bailey, L. Journal of the American Academy of Orthopaedic Surgeons 25(3), 2017
- [2] Besier, T. et al. Journal of Biomechanics 36, 1159-1168, 2003.
- [3] Ehrig, R. M., Taylor, W. R., Duda, G. N., & Heller, M. O. (2006). Journal of Biomechanics, 39(15)

Name: Dr. Andrew McDaid
Email: andrew.mcdaid@auckland.ac.nz

IMPACT OF WALKING SPEED ON JOINT ANGULAR VELOCITY

Benjamin Mentiplay¹, Megan Banky², Michelle Kahn², Ross Clark³, and Gavin Williams²
¹La Trobe University, ²Epworth HealthCare, ³University of the Sunshine Coast

INTRODUCTION

It has been shown that walking speed has an impact upon the magnitude of joint angles observed during gait (Schwartz, 2008; Winter, 1983). However, it is unknown what impact that walking speed has on joint angular velocity during gait. Understanding the angular velocity profiles during walking at various speeds may help with clinical assessments (e.g. strength or spasticity) to ensure the assessment methods match the movement speed of the lower limb observed during walking.

Therefore, the aim of the current study was to examine how lower limb joint angular velocity changes when walking at different speeds.

METHOD

A sample of 36 healthy adults were recruited (23 female, 36 ± 15 years, 170 ± 9 cm, 69 ± 12 kg). Participants underwent three-dimensional gait analysis during walking at self-selected speeds when asked to walk either at a habitual pace or a slowed pace. A modified Conventional Gait Model was used to examine the joint angles and angular velocities during walking. Data were grouped in 0.2m/s increments from 0.4 to 1.6m/s. Descriptive statistics were used to present the results for the joint angles and angular velocities at pertinent phases in the gait cycle for each walking speed.

RESULTS

The shape of the joint angular velocity profiles was consistent regardless of the walking speed. However, the magnitude of the profiles increased with increasing walking speed. Figure 1 shows the joint angular velocity profiles for each walking speed at the hip, knee and ankle. The largest joint angular velocity occurred when the knee extends during the terminal swing phase of gait, with a peak angular velocity of $384^\circ/\text{s}$ when walking between 1.4 to 1.6m/s. For the hip and ankle, the largest joint angular velocity occurred during the push off phase of gait with $220^\circ/\text{s}$ at the hip and $331^\circ/\text{s}$ at the ankle when walking between 1.4 to 1.6m/s as the leg is propelled forward for the swing phase.

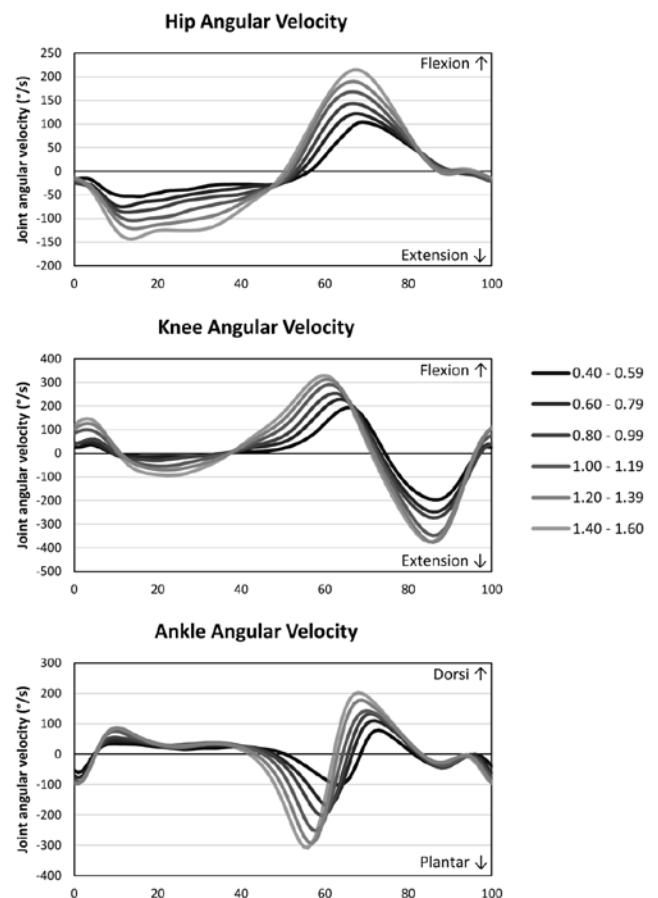


Figure 1. Joint angular velocity when walking at six different speed increments (m/s).

CONCLUSIONS

This study provides the first data on how joint angular velocity changes when walking at different speeds. This data provides a reference for patients with gait impairments. This data could also be used to ensure clinical assessment methods replicate the speed of movement observed during gait.

REFERENCES

- Schwartz, MH. J. Biomech 41, 1639-1650, 2008.
- Winter, DA. J. Mot. Behav. 15, 302-330, 1983.

Benjamin Mentiplay, b.mentipplay@latrobe.edu.au

A NETWORK MODEL FOR LUNG PARENCHYMA FOR DESCRIBING THE INTERPLAY BETWEEN THE CRUCIAL COMPONENTS OF THE EXTRACELLULAR MATRIX

Amin Iravani, Ashvin Thambyah, Kelly S. Burrowes

Department of Chemical and Materials Engineering, University of Auckland, 2-6 Park Avenue, Auckland 1023, New Zealand

INTRODUCTION

In this study, the bulk viscoelastic properties of lung tissue were modelled using a combined spring and dashpot system, and the assumption that the three main components of the extracellular matrix (ECM) are collagen, elastin and proteoglycans (PGs).

METHOD

To mimic the structure of the lung tissue alveolar network, a hexagonal model was chosen. The stress-strain behavior of the tissue is known to be non-linear. Thus in our model, the effect of the collagen and PG matrix system were assumed to consist of a non-linear spring in parallel with a Maxwell-type model (Fig 1a). To provide stability to the network, two diagonal spring elements were added within each hexagon (Fig 1b). In a way, these elements mimic the effect of the PGs' resistance to transverse compression when the tissue is axially stretched.

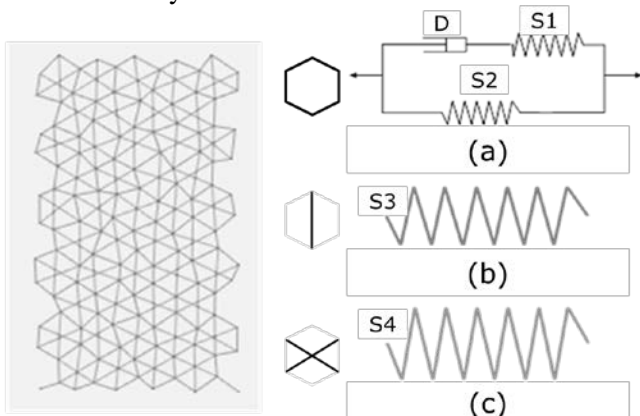


Figure 1. Hexagonal network consisting of a) a 3-element system, b) and c) single spring elements, to model the bulk response of tissue containing collagen, PGs and elastin. S1-4- Spring elements and D- Dashpot.

Finally, a vertical spring element (Fig 1c), with relatively high compliance was included in each hexagon to represent the effects of elastin during uniaxial tension of the bulk tissue. Two testing regimes were applied. Both were uniaxial extension by 30%, one with the vertical spring elements intact, and the other without. The parameters (S1-S4 and D see Fig 1) were adjusted such that the model stress-strain response fitted to the experimental data from Kononov

et al. [1]. The model was then run for the second test, without the 'elastin elements' to see if it matched the data from Kononov et al. [1] where they determined the tissue mechanical response from a rat model of elastase-induced emphysema.

RESULTS

The model's stress-strain curves are shown in comparison with the experimental data by Kononov et al. [1] (Fig. 2). Using a vertical spring element stiffness of 1.5 MPa, and an overall stiffness for the 3-element system of 300 MPa, the model prediction matched reasonably well with the experimental data. Importantly, by removing the vertical spring elements, and not changing any of the parameters, the model predictions were in good agreement with the experimental data of the elastase-treated tissue.

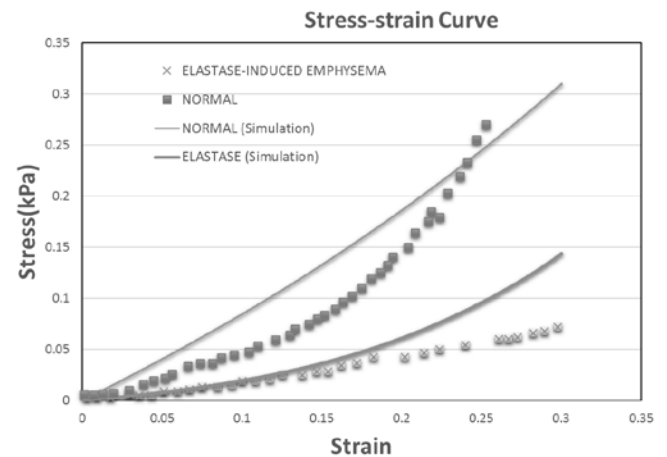


Figure 2. Comparison of the effect of elastin-degradation (elastase-treated) on measured [1] and simulated tensile stress-strain curves of lung ECM.

CONCLUSIONS

A spring-dashpot model was developed for describing the viscoelastic behavior of lung tissue at ECM level. Our modeling approach can be extended to describe the different phenomena at ECM level such as emphysema and fibrosis and ageing effect on lung function.

REFERENCES

- [1] Kononov, S. Am J Respir.Crit.Care Med. 164, 1920–1926 2001 Amin Iravani (aira902@aucklanduni.ac.nz)

MULTIVARIATE SPLINES TO ESTIMATE MUSCLE-TENDON LENGTH AND MOMENT ARMS IN THE UPPER LIMB

Thorben Pauli¹, Laura Cummack², and Thor Besier^{1,3}

¹ Auckland Bioengineering Institute, University of Auckland

² Department of Engineering, Monash University

³ Department of Engineering Science, University of Auckland

INTRODUCTION

Estimates of joint moments and muscle forces can be used to control assistive devices and monitor health or performance in workplaces or at home. They are often calculated using an underlying Hill-type muscle model. The estimation of these moments and forces requires knowledge of muscle-tendon lengths and moment arms.

While musculoskeletal modelling software such as OpenSim provides tools to compute lengths and moment arms, it is computationally expensive. Multivariate B-spline approximations have been shown to be an accurate and quick method to estimate these for lower limb muscles¹. We here test whether similar accuracy can be achieved for the upper limb.

METHOD

A generic OpenSim model of the upper limb was built by merging bodies, joints and muscles from previously published models^{2,3}.

The build-in OpenSim tool was then used to linearly scale the model to a participant's optical motion capture marker set. Optimal fibre length and tendon slack length for all muscles were optimized applying the method developed by Modenese et al.⁴.

For each muscle-tendon unit, length and moment arms were calculated for 10 discrete joint angle configurations, covering the full range of each degree of freedom. Multivariate cubic B-splines were constructed with calculated lengths and moment arms as node points.

Muscle-tendon lengths and moment arms were then interpolated for 500 discrete positions, and compared against the respective results obtained from OpenSim.

PRELIMINARY RESULTS

Multivariate B-splines were fitted to muscle-tendon length data of the biceps brachii with respect to elbow flexion and forearm pronation. The error was calculated as the difference to results from OpenSim (Figure 1).

A maximal muscle-tendon length error of 2.104×10^{-4} m was found for a nearly fully extended elbow joint and neutral forearm position, with an

overall RMSE of 4.738×10^{-5} m. The maximal moment arm error was 1.967×10^{-3} m with a RMSE of 3.138×10^{-4} m.

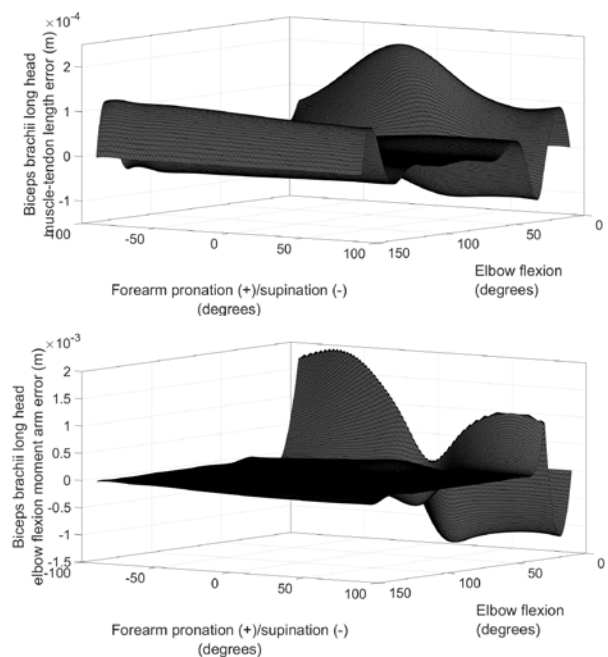


Figure 1. Errors in estimating muscle-tendon length (top) and moment arm (bottom) for the long head of the biceps brachii.

DISCUSSION

Evaluation of multivariate B-splines resulted in reasonable estimates for both, muscle-tendon lengths and moment arms in the long head of biceps brachii, while providing a computationally faster estimate compared to OpenSim's muscle analysis tool. However, it was observed that approximation errors increased significantly towards limits of the range of motion, which requires further investigation.

REFERENCES

- ¹ Sartori, M, et al.. J Biomech 45, 595 – 601, 2012
- ² Saul, K, et al.. Comput Methods Biomech Biomed Engin 18, 1445 – 1458, 2015.
- ³ Wu, W, et al.. J Biomech 49, 3626 – 3634, 2016.
- ⁴ Modenese, L, et al.. J Biomech 49, 141 – 148, 2016.

Thorben Pauli, tpau068@aucklanduni.ac.nz

PROBING THE MECHANISMS OF MUSCLE DEGENERATION IN CEREBRAL PALSY USING AGENT-BASED MODELLING

Stephanie Khuu¹, Kelley M. Virgilio², Justin W. Fernandez^{1,3}, Geoffrey G. Handsfield¹

¹Auckland Bioengineering Institute, ²Department of Biomedical Engineering, University of Virginia.

³Department of Engineering Science, University of Auckland.

INTRODUCTION

Cerebral palsy (CP) refers to a group of permanent disorders that commonly affect movement and posture. In the muscles of children with CP, structural changes include long sarcomere lengths, disorganisation of sarcomeres, reduced muscle cross-section, as well as the development of contractures [1].

The number of satellite stem cells (SSCs) in the muscle milieu plays an important role in healthy muscle regeneration. Flow cytometry methods show a decline in SSCs by ~70% in the muscles of children with contractures, compared to the muscles of typically developing children [1]. Using computational modelling, it is possible to test the levels at which loss of SSCs begin to impair muscle fibre regeneration, in healthy and disease state muscles.

Agent-based modelling (ABM) is a computational modelling technique used to represent tissue adaptation at the cellular and molecular levels [2]. Autonomous agents are situated in environments with changeable relationships. Dynamic interactions reflect complex and non-linear nature of physiological systems, and often lead to emergent phenomena. Here we demonstrate the alteration of SSC levels in an existing ABM for muscle injury and regeneration.

METHOD

The existing mouse model ABM was created in Repast Symphony, a Java-based modelling platform. The ABM was seeded using experimental studies on muscle regeneration and injury. Cellular populations in the ABM include inflammatory cells (macrophages, neutrophils, and cytokines), satellite cells, fibroblasts, and other ECM components. The ABM was displayed using a mouse muscle cross-section (Figure 1).

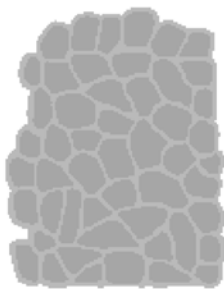


Figure 1. ABM's mouse muscle geometry was generated by masking a histological cross-section of mouse muscle, and differentiating the fibres from ECM.

SSC levels were altered by decreasing the number of SSCs per fibre between 0.25 (healthy control) and 0 (no SSCs on fibre), with a 0.05 decrement for each condition. Each SSC level was tested at baseline and

doubled levels of initial necrosis. Key model outputs included fibre and SSC cell counts as a percentage of their respective original cell counts. Each simulation represented contraction-induced muscle damage over 28 days, with each time step simulating 1 hour. The end-point percentage of original fibre count was used as a measure of muscle CSA regeneration.

RESULTS

In this model, 60% impairment in SSC count led to a 7% decline in muscle regeneration in otherwise healthy muscle and a total lack of repair in injured muscle. When initial injury was doubled, post-injury regeneration was unable to regenerate to original fibre count levels in any condition (Figure 2).

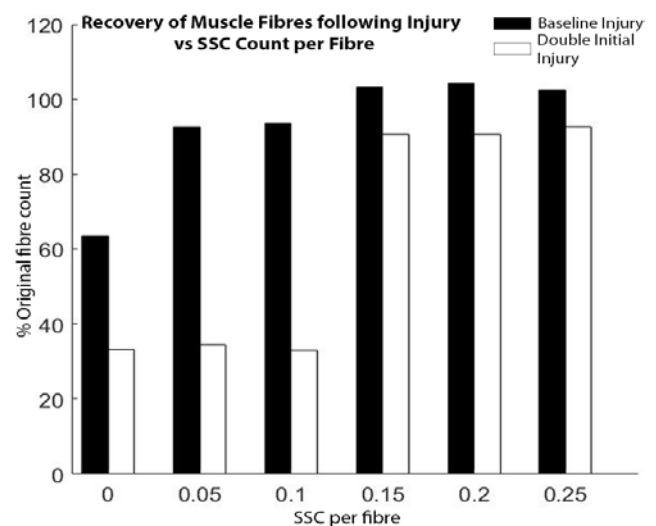


Figure 2. Baseline and double initial injury-induced muscle regeneration. Muscle fibre regeneration was impaired when the number of SSCs were ≤ 0.1 SSCs per fibre with baseline injury levels. Double initial injury-induced muscle regeneration lacked full recovery at all SSC levels, and was unable to recover at SSC levels ≤ 0.1 SSCs per fibre.

CONCLUSIONS

ABM was utilized as a tool to explore hypotheses regarding the cellular pathophysiology of CP. Specifically, we were interested in simulating the degree of SSC loss required to reach a pathological lack of muscle regeneration. In this simple model, we explored the relationship of just one cell (SSC) on recovery of muscle fibre count post-injury. We will expand on this work by further developing the model and including a more comprehensive set of altered cells and cytokines consistent with the myocellular environment in CP.

REFERENCES

- [1] H. K. Graham et al., *Nat. Rev. Dis. Prim.*, 2, 2016.
- [2] T. E. Gorochofski, *Essays Biochem.*, 60, 325–336, 2016.

VALIDATION OF THREE WORKFLOWS TO OBTAIN BONE AND CARTILAGE MESHES FOR COMPUTATIONAL HUMAN KNEE MODELLING

Nynke Rooks¹, Mousa Kazemi¹, Marco T. Y. Schneider¹, Thor Besier¹
¹Auckland Bioengineering Institute, Auckland, New Zealand

INTRODUCTION

Computational knee modelling and simulation can be used to investigate, in a low cost and prompt manner, personalized knee mechanics and has potential for clinical application. However, the grand knee challenge showed that the outputs of different computational models, created using the same set of data, varied significantly,¹ bringing the reproducibility of computational models into question.² Decisions made in modelling workflows, while based on objective scientific principles, commonly rely on the intuition, experience, and knowledge of the modeler, and therefore, may affect the reproducibility of models.

The first steps to build a computational knee model are image segmentation and mesh generation. The aim of this study was to investigate the effect that differences in segmentation and mesh generation workflows have on the geometries obtained.

METHOD

The bones and cartilage from a T2 weighted sagittal plane MRI dataset of a knee (Natural Knee data, Denver University) were segmented 3 times by the author and once by a co-author using a custom MATLAB script. The intra- and inter-rater accuracy of segmentation was determined by comparing the mean cloud-to-cloud distance. Using one segmentation, three existing workflows that used a statistical shape model³ (SSM) for mesh generation were compared: Principal Component regression (PCR), Principal Component + local fit (PC+local fit),⁴ and Partial Least Square Regression (PLSR). The regression matrix (X) used in PCR and PLSR contained demographic parameters (age, gender, height, weight, and BMI), cartilage thickness fields, and the projected weights of 5 principal components of the bone shapes. The mean cloud-to-cloud distance between the meshes and segmentations were calculated.

RESULTS

Our preliminary results show that inter-rater distances were larger than the intra-rater distance (Table 1), especially in the patella cartilage (mean error = 1.044 mm). No significant differences were found between the meshes obtained from the different workflows (Figure 1).

Table 1: Mean segmentation distances (mm) (\pm SD)

	Bone	Cartilage
Intra-rater	0.363 \pm 0.025	0.308 \pm 0.079
Inter-rater	0.457 \pm 0.060	0.592 \pm 0.320

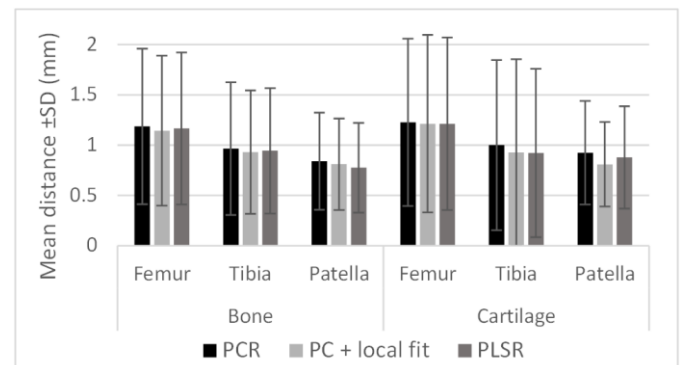


Figure 1: Mean distance between mesh and segmented point clouds

CONCLUSIONS

All three workflows appear to provide meshes with similar quality. This suggests that the choice of workflow does not affect the obtained geometry significantly. We hypothesize that this is due to the use of the SSM which informed all three mesh generating workflows. Further work should investigate the effect of the small differences, between the meshes obtained from the workflows, on the simulated knee kinematics.

The inter-rater segmentation cartilage distance is larger than the intra-rater distance, suggesting difficulties in manual cartilage segmentation. An automatic SSM based segmentation tool could be used to reduce human error.

REFERENCES

- ¹ Fregly, B.J., Journal of Orthopaedic Research 30(4), 503-513, 2012
- ² Erdemir A, 2018 IMAG Futures Meeting – Moving Forward with the MSM Consortium, 2018
- ³ Kazemi, M., Unpublished doctoral thesis, University of Auckland, 2018
- ⁴ Zhang, J., CMBBE: Imaging & Visualization 2(3), 176-185, 2014

ACKNOWLEDGEMENTS

This work was supported by the National Institutes of Health (Grant No. R01Eb024573).

Nynke Rooks – nroo469@aucklanduni.ac.nz

THE EFFECT OF SPLINT TYPE ON THE STRESS DISTRIBUTION OF BRUXISM PATIENT'S TEETH

Satrio Wicaksono¹, Aldilla Miranda², Tatacipta Dirgantara¹ and Andi Isra Mahyuddin¹

¹Faculty of Mechanical and Aerospace Engineering, Institut Teknologi Bandung

²Periodontology Department, Faculty of Dentistry, Universitas Padjadjaran

INTRODUCTION

Bruxism is considered as a para-functional problem, which is defined as form of movement that consisted of clenching, grinding and gnashing of the teeth and usually occurs without self-awareness [1]. One of the available method to prevent bruxism is by using night guard or occlusal splint [2]. Commercially available occlusal splints can be divided into three different types: hard, soft and dual laminated splints. In the current study, the effectiveness of hard, soft and dual laminated splints to prevent tooth failure at the time of bruxism will be studied in detail.

METHOD

The effectiveness of splint in preventing tooth failure can be observed from the teeth's stress at the time of bruxism. In the current study, finite element method is used to obtain the stress distribution of the teeth. Previously, a finite element study on the effectiveness of hard acrylic splint has been performed [3]. Unfortunately, contact problem was occurred due to mismatched mesh between two contacted area, i.e., teeth (enamel) and splint. In the current study, the contact problem has been solved by performing shared topology to ensure matching surface and mesh between contacted areas. The final model used in this study is shown in Figure 1.

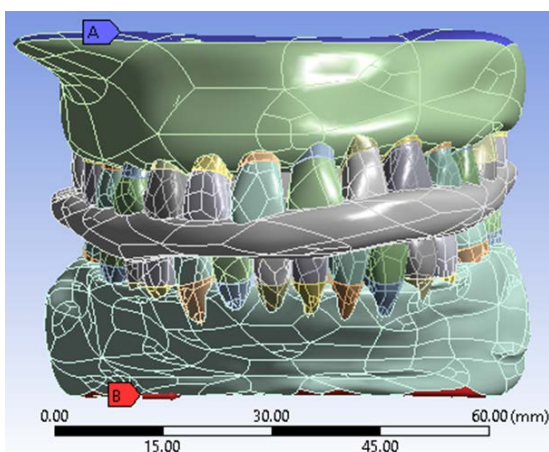


Figure 1. The final finite element model.

To check the splint's effectiveness, the teeth's stress distributions with hard, soft and dual laminated splints are then compared with the teeth's stress distribution without splint which has been obtained in the previous study [4].

RESULTS

The result obtained from the previous study show that teeth's maximum principle stress without splint is 160 MPa, which is way higher than the tooth strength of 98 MPa [4]. The hard and soft splints performed similarly well to prevent tooth failure as the teeth's maximum principle stress are reduced to 8.78 MPa and 7.97 MPa respectively. The dual laminated splint performed slightly worse as the teeth's maximum principle stress reaches 12.6 MPa at the location shown in Figure 2.

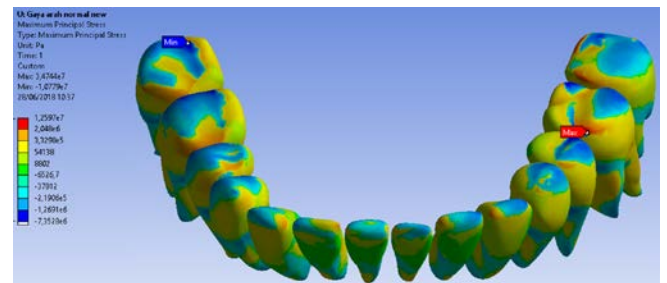


Figure 2. Maximum principle stress distribution of mandible teeth with dual laminated splint.

CONCLUSIONS

Hard, soft and dual laminated splints have shown to be able to prevent tooth failure at the time of bruxism as the maximum principle stress results are still way lower than tooth's maximum strength. The finite element results also show that the hard and soft splints performed similarly well and the dual laminated splint performed slightly worse in comparison to the other two splints.

ACKNOWLEDGEMENT

The author acknowledges the help of Dwi Mulyaningsih and Yadi Ferdian in this research. The author also gratefully acknowledges Kementerian Riset Teknologi, dan Pendidikan Tinggi Republik Indonesia for the PDUPT research grant.

REFERENCES

1. Ruppelch, DR. 2004. J Clin Update; 26(1):25-27.
2. A. Johansson, et al. Journal of Prosthodontic Research, 55:127-136, 2011.
3. S. Wicaksono et al. ISB 2017, Brisbane, Australia, 2017.
4. A. S. Budiaman et al. AP Biomechanics 2015, Sapporo, Japan, 2015.

Speaker: Satrio Wicaksono, satriowicaksono@ftmd.itb.ac.id

MAP-OPENSIM MODEL HIP MUSCLES' PATHWAYS DETERMINED USING OPTIMIZED WRAPPING SURFACES

¹Simao Brito da Luz, ¹Bryce A. Killen, ¹David J. Saxby, ²Alex D. Carlton, ²Thor F. Besier, ¹David G. Lloyd

¹GCORE, Menzies Health Institute Queensland, Griffith University, Australia

²ABI, University of Auckland, New Zealand

INTRODUCTION

Generic musculoskeletal (MSK) models use via points and 3D wrapping surfaces to constrain musculotendon (MTU) pathways. However, when generic models are individually scaled, MTU pathways can penetrate bones, and have discontinuous MTU lengths and moment arms, producing inaccurate predictions of MTU and joint contact forces [1]. For these reasons, building MSK models can be a slow manual process that is tedious and error prone.

The Musculoskeletal Atlas Project (MAP) can automatically create personalized OpenSim MSK models using motion capture and/or sparse medical imaging data [2]. We now describe a new method to automatically generate and optimize wrapping surfaces that constrain hip MTU pathways to be continuous, follow the patterns of published MTU lengths and moment arms and without penetrating bones.

METHOD

An OpenSim-MAP model was generated, with MTU insertions and origins adjusted using a SOMSO model. MTU wrapping surfaces, i.e., cylinders, spheres or tori, were automatically defined and fitted to delineated bone surfaces defined in MAP. Tori had initial: 1) rotations aligned with XZ plane, 2) centers matching OpenSim gait2392 generic model's via points, and 3) outer and inner radius equal 0.02 and 0.019 respectively.

Wrapping surfaces geometric parameters were tuned via Multi-Objective Particle Swarm Optimization to ensure: 1) continuous hip flex-extension, int-external and add-abduction MTU moment arms vs. hip flexion, 2) no MTU penetration into bones, 3) match patterns of MTU lengths and moment arms to those from OpenSim generic models and experimental studies and 4) minimize difference between tori centers and initial via points. Pearson's correlations (ρ) were calculated between optimized MAP-OpenSim model's MTU lengths and hip moment arms with those from generic models and experimental studies.

RESULTS

Hip MTU lengths and moment arms were continuous and similar to those from generic models and experimental studies. High correlations were found

between optimized and experimental and generic MTU moment arms (all with $\rho > 0.53$ and $p < 0.001$) and between MTU lengths and experimental studies (all with $\rho > 0.8$ and $p < 0.04$). Furthermore, optimization prevented MTU bone penetration, and small differences between optimized tori centers and OpenSim generic model's via points ($< 1 \pm 0.7$ cm).

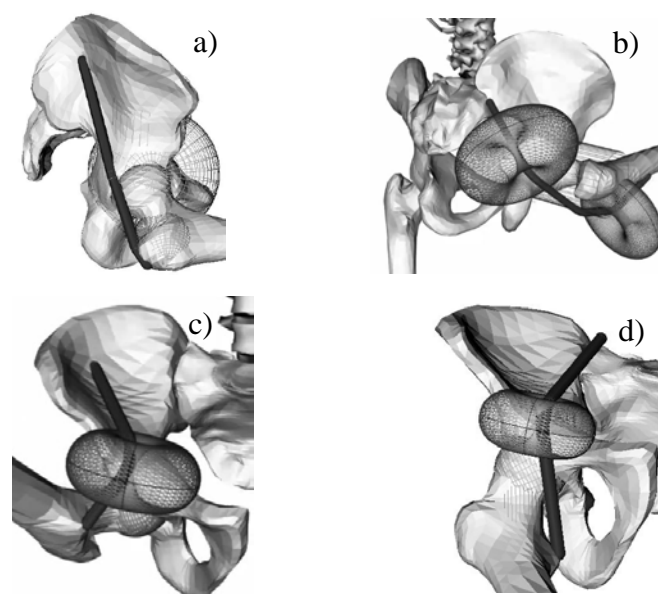


Figure 1. Fig.1: Optimized wrapping surfaces constraining MAP-OpenSim hip MTU pathways: a) glut med, b) glut max (2nd fibres), c) iliacus, and d) psoas

CONCLUSIONS

We have shown that hip MTU pathways and wrapping surfaces can be automatically generated from the personalized MAP-OpenSim MSK models. Therefore, these models can be readily morphed to each individual's sparse imaging data, potentially improving estimates of MTU and joint contact forces during dynamic simulations.

REFERENCES

- [1] Fregly, B.J., et al., (2012). J. Orthop. Res, 30:503-513
- [2] Zhang, J., et al., (2014). ISBMS 2014, 8790:182-192

Speaker: Simao Brito da Luz (s.britodaluz@griffith.edu.au)

OPENSIM-COMPATIBLE LIBRARY FOR KINEMATIC RECONSTRUCTION USING INERTIAL MEASUREMENT UNITS

Ted Yeung¹ and Thor Besier^{1,2}

¹Auckland Bioengineering Institute, University of Auckland

²Department of Engineering Science, University of Auckland

INTRODUCTION

Human motion and bioelectric signals are essential to assess and monitor health and athletes' performance as well as informing design and controlling assistive devices in the workplace or at home. Traditional methods collect data in a restricted, controlled environment. The advent of wearable technologies, such as miniature, wireless inertial measurement units (IMUs), is enabling the measurement of human motion in the real world, opening up new possibilities for biomechanical applications¹.

Reconstructing human kinematics from the IMUs is challenging and requires a complex pipeline that interprets inertial data and converts these to kinematic predictions, typically with the aid of a kinematic model. OpenSim is a popular, open source musculoskeletal modelling tool that provides a framework to create kinematic models, but as yet, does not support motion reconstruction from IMUs. We present here a new library for using OpenSim models together with IMU data to reconstruct human kinematics.

METHOD

Our proposed library (Figure 1) consists of three modules:

1. IMU data Module (IMU I/O)
2. OSIM Module (Model Parser)
3. Inverse Kinematics Module

The IMU data module reads in the IMU data either from a data file or stream via USB or Bluetooth then passes it to the kinematics module.

The OSIM module reads in a OpenSim model file and creates a data structure that allows for model parameters from OpenSim to be used in the custom inverse kinematics module.

The inverse kinematics module reconstructs joint kinematics based on the model parameters and IMU data. The module features two modes of operation:

- 1) Quaternion difference tracking
- 2) IMU-based inverse kinematic optimisation

The Quaternion tracking is quick, which allows for real time tracking of the body segments. While the IMU-based non-linear least squares inverse kinematic

optimisation provides a more accurate representation of the joint angle for the given IMU data.

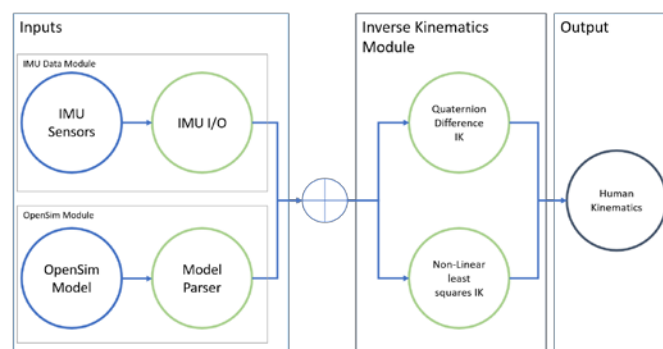


Figure 1. Overview of the processing module

The output of the library are the generalised coordinates consistent with the OpenSim model, stored as a motion file (.mot), which can also be visualised in OpenSim.

RESULTS

We tested this library on a 6 degrees of freedom (DoF) synthetic IMU data set on a simplified 6 DoF gait model and an 8 DoF upper limb model. The preliminary results for the gait model was an estimated max drift 0.02 m/s and 0.06 °/s, while for the upper limb model the was a maximum drift of 1 °/s during dynamic motion.

DISCUSSION

Wearable sensors provide an opportunity to capture human motion outside the lab, with many interesting applications. The integration of IMUs with OpenSim allows OpenSim users to use the vast collection of existing .osim models to reconstruct kinematics.

Another advantage of this library is the exposure to other tools within OpenSim, such as inverse dynamics and muscle analysis, which are not offered by other IMU-based kinematic tools.

REFERENCES

1. IMeasureU homepage (retrieved 21 June 2018) <https://imeasureu.com/>
2. Delp, S.L., IEEE T Bio-Med Eng, 54(11), 1940-1950, 2007

Ted Yeung, tyeu008@aucklanduni.ac.nz

A COMPARISON OF FOUR FACTORIZATION METHODS FOR MUSCLE SYNERGY EXTRACTION

Mohammad Fazle Rabbi¹, Claudio Pizzolato¹, Laura Diamond¹, Chris Carty^{1,2}, David G. Lloyd¹

¹GCORE, Menzies Health Institute Queensland, Griffith University, Gold Coast, Australia

²Children's Health Queensland Hospital and Health Service, Brisbane, Australia

INTRODUCTION

The human central nervous system may simplify the control of motor tasks via the coordinated activation of groups of muscles known as muscle synergies. Several matrix factorization methods (FM) can be applied to extract synergies from electromyographic (EMG) signals acquired during specific motor tasks. The most commonly used FM are: (1) principal component analysis (PCA); (2) independent component analysis (ICA); (3) non-negative matrix factorization (NNMF); and (4) factor analysis (FA). Each method has advantages within a given set of constraints and applications. Specifically, PCA and FA assume the source signal to be Gaussian distributed while ICA assumes the source to be strictly non-Gaussian. However, there is no specific assumption for NNMF (Tresch 2006). Similarly, each of the FM make assumptions regarding noise distribution. Performance of a FM depends on the signal-to-noise ratio (SNR), in addition to residual noise in the muscle excitations following traditional low-pass filtering (Ebied et al. 2018). It is important to see how FM perform under different noise conditions because synergy extracted from EMG signal is also prone to noise and artifacts. It is unclear what FM is most appropriate for muscle synergy extraction during walking under a specific source and noise distribution. The aim of this study was to determine which synergy extraction FM is most appropriate when using muscle activation patterns acquired during walking and applying different noise distributions and signal-to-noise ratios.

METHOD

EMG data was recorded from one healthy individual. The subject was asked to walk on an instrumented treadmill at a slow (0.8 m/s), medium (0.88 m/s) and fast (1.04 m/s) speed for 15s each. Three trials were collected for each of the three speed conditions. The EMG data was collected from 12 major muscles of the dominant (right) leg using wireless sensors (1000Hz). Data was band-pass filtered (30-400 Hz), full wave rectified, and low-pass filtered (6 Hz) using a zero lag 4th order Butterworth filter. Data was normalized to peak amplitude for each muscle.

To generate noise, SNR ranges were fixed from -5 dB to 15 dB. Based on the noise power, additive white Gaussian noise and band-limited Rayleigh distributed (non-Gaussian) noise were generated. EMG envelopes

were mixed with the noise prior to apply the FM for synergy extraction. MATLAB functions *pca()*, *nnmf()* and *factoran()* were used to implement PCA, NNMF and FA methods, respectively. ICA was implemented according to Hyvarinen et al. (2000). Variance accounted for (VAF) was calculated after muscle excitations were reconstructed using four synergy vectors and synergy activations.

RESULTS

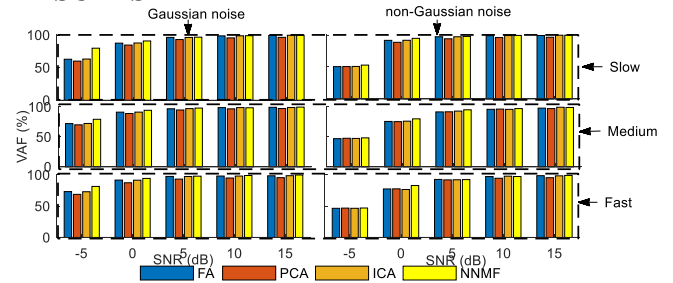


Figure 1. Muscle reconstruction performance of four factorization methods for three walking speeds.

VAF (%) of the four FM for each of the three walking speeds (slow, medium and fast) and all five SNRs (-5, 0, 5, 10 and 15 dB) are displayed in Figure 1. In general, VAF for all FM augments as the signal power intensifies in all noise and walking speed conditions. The performances of the four methods remain similar using Gaussian noise but deteriorates significantly when high non-Gaussian noise is applied. The VAF performance of the four FM remain consistent across walking speeds. Among all FM, NNMF appears to have better performance in three different walking speeds and in both noise scenarios. PCA was most sensitive to the presence of noise compared to the other FMs.

CONCLUSIONS

This study compared the performance of four synergy extraction methods during walking. Our results show that NNMF is less sensitive to noise than the other methods assessed. Therefore, NNMF may be preferable synergy extraction in cyclic lower limb tasks, such as walking.

REFERENCES

- Ebied, Ahmed et al. Medical Engineering and Physics, 1-0, 2018.
 - Hyvarinen, A, et al. Neural Networks 13, 411–30, 2000.
 - Tresch, M. C. Journal of Neurophysiology 95, 2199–2212, 2006.
- Mohammad Fazle Rabbi fazle.rabbi@griffithuni.edu.au

MAGNETIC RESONANCE IMAGING AND FREEHAND 3D ULTRASOUND METHODS PROVIDE SIMILAR ESTIMATES OF FREE ACHILLES TENDON GEOMETRY

Daniel Devaprakash¹, Claudio Pizzolato¹, Rod S. Barrett¹, Steven J. Obst², Ben Kennedy¹, Kahlee L. Adams³, Adam Hunter³, Nicole Vlahovich³, David L. Pease³, David G. Lloyd¹

¹ GCORE, Menzies Health Institute Queensland, Griffith University, Gold Coast, Australia

²School of Health, Medical, and Applied Sciences, Central Queensland University, Bundaberg, Australia

³Movement Science, Australian Institute of Sport, Canberra, Australia

INTRODUCTION

Personalised computational models of the Achilles tendon (AT) are required for non-invasive estimates of localised AT strain during common locomotor and rehabilitation tasks (Pizzolato et al. 2017). Two characteristics of personalisation include AT geometry and AT material properties (Hansen et al. 2017). The purpose of this study is to assess if similar estimates of free AT geometry and shape can be obtained when using novel magnetic resonance imaging (MRI) methods and previously established freehand 3D ultrasound (3DUS) methods (Obst et al. 2013).

METHODS

Three elite middle distance runners (22 ± 3.7 yrs, 61.7 ± 6.2 kg) with no prior history of AT injury participated in the study. Participants refrained from strenuous physical activity in the 24 hours prior to testing. Following AT preconditioning (Hawkins et al. 2009), participants underwent MRI scans of their free AT using a Philips Ingenia 3.0T MR scanner. High resolution (hi res) ankle joint MRI (T1W 3D FFE, TR/TE 8.0/4.1 ms) and subtraction ultrashort echo time (SUTE) sequences were used to image the free AT at rest. Hi res ankle joint scans were acquired in the sagittal plane with the ankle in neutral position; the slice thickness and slice gap were 0.6 mm and 0.3 mm respectively. SUTE scans were acquired in the axial plane with the ankle at approximately 30° plantarflexion; the slice thickness and slice gap were 4 mm and 2 mm respectively. The AT was subsequently scanned using a 3DUS method by sweeping the instrumented ultrasound transducer (Canon PLT-805) along the free AT, while motion capture data were recorded synchronously using an 8-camera Vicon motion capture system. 2D ultrasound images and motion capture data were acquired at 30 Hz and 100 Hz respectively. To mimic MRI scans, 3DUS images were acquired with the ankle in two positions, neutral and 30° plantarflexion. MRI and 3DUS slices were then segmented using Stradwin software (Version 5.3). Estimates of free AT volume, average cross-sectional area, and length were compared between the MRI and 3DUS methods. Shape similarity was assessed using Jaccard index (JI) and Hausdorff distance (HD).

RESULTS

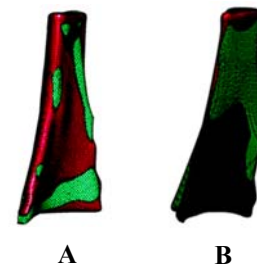


Figure 1: 3D reconstruction of the free AT using (A) high resolution ankle MRI (green) and freehand 3DUS (magenta) at neutral ankle angle, and between (B) SUTE (green) and 3DUS (magenta) method at 30° plantarflexion.

Overall a high level of similarity was achieved between MRI and 3DUS methods (Figure 1 and Table 1).

Table 1: Comparisons between MRI and 3DUS methods.

	Neutral position		30° Plantarflexion	
	Hi res ankle MRI	3DUS	SUTE	3DUS
Vol. (ml)	3.7±0.5	3.7±0.5	3.8±0.6	3.7±0.6
Avg. CSA (mm ²)	71.9±2.9	71.1±3.3	72.4±4.0	72.7±1.8
Length (mm)	51.8±4.7	51.7±6.7	51.9±6.9	50.5±7.3
JI	0.8±0.02		0.6±0.02	
HD	0.007±0.001		0.014±0.004	

CONCLUSIONS

Preliminary analysis suggests that 3DUS and MRI methods provide similar estimates of free AT geometry. Data analysis from 20 elite middle distance runners is currently being performed, and image processing methods are currently being applied to identify Achilles sub-tendon twist in vivo.

REFERENCES

- Pizzolato et al Front Comput Neurosci 11, 96, 2017
- Hansen et al Biomech 56, 26-31, 2017
- Obst et al J App Phys 116, 376-384, 2013
- Hawkins et al Biomech 42 2813-2817, 2009
- Daniel Devaprakash daniel.devaprakash@griffithuni.edu.